Journal Pre-proofs

The chemical origin of temperature-dependent lithium-ion concerted diffusion in sulfide solid electrolyte $Li_{10}GeP_2S_{12}$

Zhong-Heng Fu, Xiang Chen, Nan Yao, Xin Shen, Xia-Xia Ma, Shuai Feng, Shuhao Wang, Rui Zhang, Linfeng Zhang, Qiang Zhang

PII: S2095-4956(22)00027-4
DOI: https://doi.org/10.1016/j.jechem.2022.01.018
Reference: JECHEM 2351

To appear in: *Journal of Energy Chemistry*

Received Date: 19 December 2021
Revised Date: 13 January 2022
Accepted Date: 16 January 2022

Please cite this article as: Z-H. Fu, X. Chen, N. Yao, X. Shen, X-X. Ma, S. Feng, S. Wang, R. Zhang, L. Zhang, Q. Zhang, The chemical origin of temperature-dependent lithium-ion concerted diffusion in sulfide solid electrolyte $Li_{10}GeP_2S_{12}$, *Journal of Energy Chemistry* (2022), doi: https://doi.org/10.1016/j.jechem.2022.01.018

The chemical origin of temperature-dependent lithium-ion concerted diffusion in sulfide solid electrolyte $Li_{10}GeP_2S_{12}$

Zhong-Heng Fu[a], Xiang Chen[a,*], Nan Yao[a], Xin Shen[a], Xia-Xia Ma[a], Shuai Feng[a,b], Shuhao Wang[a,c], Rui Zhang[d], Linfeng Zhang[e,f], Qiang Zhang[a,*]

[a] *Beijing Key Laboratory of Green Chemical Reaction Engineering and Technology, Department of Chemical Engineering, Tsinghua University, Beijing 100084, China*
[b] *College of Chemistry and Chemical Engineering, Taishan University, Taian 271021, Shandong, China*
[c] *School of Chemistry, The University of New South Wales, Sydney NSW 2052, Australia*
[d] *School of Materials Science and Engineering & Advanced Research Institute of Multidisciplinary Science, Beijing Institute of Technology, Beijing 100081, China*
[e] *DP Technology, Beijing 100080, China*
[f] *AI for Science Institute, Beijing 100080, China*

[*]**Corresponding author.**
E-mail address: xiangchen@tsinghua.edu.cn (X. Chen),
zhang-qiang@mails.tsinghua.edu.cn (Q. Zhang)

ABSTRACT

Solid-state batteries have received increasing attention in scientific and industrial communities, which benefits from the intrinsically safe solid electrolytes (SEs). Although much effort has been devoted to designing SEs with high ionic conductivities, it is extremely difficult to fully understand the ionic diffusion mechanisms in SEs through conventional experimental and theoretical methods. Herein, the temperature-dependent concerted diffusion mechanism of ions in SEs is explored through machine-learning molecular dynamics, taking $Li_{10}GeP_2S_{12}$ as a prototype. Weaker diffusion anisotropy, more disordered Li distributions, and shorter residence time are observed at a higher temperature. Arrhenius-type temperature dependence is maintained within a wide temperature range, which is attributed to the linear temperature dependence of jump frequencies of various concerted diffusion modes. These results provide a theoretical framework to understand the ionic diffusion mechanisms in SEs and deepen the understanding of the chemical origin of temperature-dependent concerted diffusions in SEs.

Keywords: Solid-state batteries; Solid electrolytes; Concerted diffusion; Machine-learning molecular dynamics

1. Introduction

Inorganic solid electrolytes (SEs) have been widely and strongly considered for building safe and high-energy-density next-generation lithium (Li) batteries due to their intrinsic safety and high compatibility with high-capacity electrodes [1–4]. Tremendous SEs have been explored to improve their ionic conductivity, anodic and cathodic stabilities, and mechanical properties. In general, routine inorganic SEs can be divided into three class, i.e., oxide (e.g., garnet $Li_7La_3Zr_2O_{12}$ (LLZO) [5], NASICON $Li_{1.5}Al_{0.5}Ti_{1.5}(PO_4)_3$ (LATP) [6], perovskite $Li_{0.5}La_{0.5}TiO_3$ [7]), sulfide (e.g., thio-LISICON $Li_{10}GeP_2S_{12}$ (LGPS) [8], argyrodite Li_6PS_5X (X=Cl, Br, and I) (LPSX) [9], glass ceramics Li_3PS_4 and $Li_7P_3S_{11}$ (LPS) [10,11]), and halide SEs (Li_3MX_6 (M=Y, Er, and In, X=Cl, Br, and I) [12]). Compared with oxide and halide SEs, sulfide SEs exhibit higher ionic conductivities, which are attributed to the larger polarizability of anion S^{2-} [13,14]. Especially, LGPS exhibits an exceptionally high ionic conductivity of 12 mS cm^{-1} at room temperature, comparable to that of routine organic liquid electrolytes [8]. Consequently, a comprehensive and deep understanding of the ionic migration mechanism in the LGPS lattice is of enormous interest to enable a rational material design of new SEs with high ionic conductivities.

SEs exhibit the collective dynamics of Li ions similar to that in supercooled glass-forming liquids [15,16], which is different from routine solid materials where the mobile ions individually hop between crystallographic sites. Two characteristic cooperative mechanisms were proposed to understand the dynamics behavior, namely, Li–Li correlation (normally named concerted diffusion) [17–19] and Li–polyhedron framework correlation (i.e., paddle-wheel effect) [20,21]. Such correlations flatten the energy landscape of the Li-ion migrations in the framework and thus significantly reduce the activation energy, which has been believed to be the origin of fast ion

diffusion in SEs [19]. Especially, concerted diffusion is of general significance to contribute to high ionic conductivities in various SEs compared to the paddle-wheel effect usually found in glassy SEs [20]. Although Li-ion diffusion pathways and diffusion barriers have been successfully characterized by neutron diffraction techniques [22] and transition state theory calculations [23], it is challenging to intuitively understand concerted diffusions and provide a quantitative description regarding concerted diffusion mechanisms [24].

The temperature dependence of ionic diffusivities in SEs is practically critical because the operating temperature is set at low or high temperatures (e.g., −50 to 200 °C or higher) [13], which stimulates scientific interest in the temperature-dependent concerted diffusions. Intuitively, ionic motions become more frequent at higher temperatures. A stronger mutual effect between the motions is supposed based on stronger phonon-phonon interactions with an increasing temperature [25], which can result in changed diffusion modes at different temperatures. However, it is extremely difficult to directly probe the concerted diffusions at different temperatures.

Molecular dynamics (MD) can simulate the time evolution of atomic positions, enabling the direct observations of concerted diffusions. Unfortunately, it is difficult to get access to a precise description of interatomic interactions. Only a simulation duration of hundreds of picoseconds and a simulation size of hundreds of atoms are allowed in the accurate but time-consuming *ab initio* molecular dynamics (AIMD) simulations [26]. Empirical parameter fittings in large-scale classical MD (CMD) restrict the accuracy of the simulation. Machine-learning molecular dynamics (MLMD) merges the advantages of AIMD and CMD, significantly accelerating the simulation without the loss of accuracy. Therefore, MLMD has been strongly

considered as one of the most promising approaches to probe the ionic dynamics in SEs [27].

In this contribution, the temperature-dependent concerted diffusions are comprehensively investigated by deep potential molecular dynamics (DPMD), which is an emerging neural network (NN)-based MLMD [26,28–30] and has been widely used in probing solvation structures [31], ionic diffusions [27], phase transitions [32], interfacial reactions [33], etc. The DPMD method exhibits several advantages over the other MLMD methods. (1) Less manual intervention: Only atomic types and coordinates need to be manually input. (2) The framework is compatible with both isolated molecules and periodic systems. (3) NNs are used in both filter networks and computing networks. LGPS is adopted as a model system because of the significant research interest stemming from its high ionic conductivity. Although more isotropic ionic diffusivities, more disordered Li-ion distribution, and shorter averaged residence time are observed at higher temperatures, the ionic diffusivity of LGPS follows Arrhenius-type temperature dependence. The Arrhenius-type temperature dependence is attributed to the linear temperature dependence of jump frequencies of various concerted diffusion modes. These findings offer a fundamental understanding of the temperature-dependent ionic diffusion mechanism in SEs.

2. Experimental

2.1. Deep potential training

Deep Potential Generator (DP-GEN) [34] interfaced with Vienna *Ab initio* Simulation Package (VASP) [35], DeePMD-kit [36], and Large-scale Atomic/Molecular Massively Parallel Simulator(LAMMPS) [37] were adopted for an automatic training framework towards deep potential. The initial crystalline structure of LGPS was obtained from the high-throughput computational database Materials

Project [38]. The lattice constant of LGPS was fixed to the experimental result (i.e., a=b=8.71 Å, c=12.61 Å, space group: $p\bar{4}m2$) [39] in all simulations. A detailed training protocol is listed below.

(1) After a careful structural optimization, AIMD simulations using VASP [40] were performed in 20 slightly distorted LGPS structures consisting of 400 atoms (i.e., a supercell of $2 \times 2 \times 2$), which is based on the following considerations. (1) A faster energy and force convergence was found in a larger simulation size regarding the LGPS system, similar with the previous report [41]. (2) The artificial mirror force induced by the periodic boundary condition decays significantly in a large simulation size. A minimal Γ point was used for the k-point sampling. The kinetic cutoff was set to 400 eV for the plane wave expansion. The criterion for electronic convergence is set to 10^{-6} eV.

(2) Dataset including atomic configurations, energies, and forces, which were extracted from the AIMD simulations, were constructed for deep potential training. Deep neural network (DNN) training was performed employing DeePMD-kit, in which four independent models were used. The sizes of {25, 50, 100} and {240, 240, 240} were used for the embedding and fitting network, respectively. The radical cutoff is set to 6 Å, which was demonstrated to be large enough to ensure the locality of the deep potential [42].

(3) MD simulation tests were performed using LAMMPS to evaluate the force deviation of the configurations in the trajectories among four trained models. Canonical ensemble (NVT) with a Nose-Hoover thermostat [43,44] was adopted in the MD simulation, in which a series of simulation temperatures (i.e., 250, 300, 400, 500, 600, 800, 1000, and 1200 K) were used to ensure the accuracy at a wide range of temperatures. The simulation time was set to 60 ps. The configurations with force

deviations between 0.12 and 0.25 eV $Å^{-1}$ were screened out and were added to the dataset for the next iteration of training.

(4) Twelve iterations of DNN training and MD simulation tests were performed. Finally, the percentage of the configurations with force deviations less than 0.12 eV $Å^{-1}$ is 99.73%. Using 1000 configurations randomly selected from the dataset for a test of deep potential, the energy and force root-mean-square errors (RMSEs) are 0.42 meV $atom^{-1}$ and 46 meV $Å^{-1}$, respectively (Fig. S1). This result demonstrates the reliability of our DP potential.

2.2. Molecular dynamics simulations

All temperature-dependent MD simulations were performed using LAMMPS. The parameters similar to that in deep potential training were used except for a longer simulation time of 40 ns. A constant-heating-rate annealing step from 100 K to target temperature was performed within 50 ps before the diffusion sampling steps.

The ionic diffusivity *D* was determined based on the random walk model [45]

$$D = \lim_{t\to\infty}\left[\frac{\langle[\vec{r}(t)]^2\rangle}{2dt}\right], \quad (1)$$

where *d* is the dimensionality of the diffusion, *t* the time, and $\langle[\vec{r}(t)]^2\rangle$ is the averaged mean square displacement (MSD) overall Li atoms,

$$\langle[\vec{r}(t)]^2\rangle = \frac{1}{N}\sum_{n=1}^{N}\langle[\overrightarrow{r_n}(t+t_0)]^2 - [\overrightarrow{r_n}(t_0)]^2\rangle, \quad (2)$$

where $\overrightarrow{r_n}(t)$ is the displacement of the n^{th} Li atom at time *t*. The total MSD $N\langle[\vec{r}(t)]^2\rangle$ is used to evaluate a sufficient diffusion event sampling.

The size-dependent ionic diffusivities were determined in a series of cell sizes of $1\times1\times1$, $1\times1\times2$, $2\times2\times1$, $2\times2\times2$, $3\times3\times2$, $3\times3\times3$, $4\times4\times2$, $4\times4\times3$ and $5\times5\times2$, corresponding to the atom numbers of 50, 100, 400, 800, 900, 1350, 1600, 2400 and 2500, respectively, in which the simulation temperature was fixed at 300 K. The temperature-dependent ionic diffusivities were determined at 250,

275, 300, 325, 350, 400, 450, 500, 600, 800, 1000, and 1200 K.

The Li-ion probability densities, radial distribution functions, and Van Hove correlation functions were determined by the pymatgen-analysis-diffusion package [46], which is an add-on to pymatgen for diffusion analysis [47]. Van Hove correlation functions $G(\vec{r},t)$ is defined as the probability of finding a particle at position $\vec{r}$ at time *t* on the basis of the particle at the origin at initial moment *t*=0,

$$G(\vec{r},t) = \frac{1}{N}\langle\sum_{i=1}^{N}\sum_{j=1}^{N}\delta\left(\vec{r}+\vec{r}_j(0)-\vec{r}_i(t)\right)\rangle, \quad (3)$$

where $\langle\cdot\rangle$ and $\delta(\cdot)$ denote an ensemble average and a three-dimensional Dirac delta function, respectively. The Van Hove correlation functions are usually divided into two terms, "self" and "distinct" parts, by discriminating between the cases $i=j$ and $i\neq j$, respectively.

$$G(\vec{r},t) = \frac{1}{N}\langle\sum_{i=1}^{N}\delta\left(\vec{r}+\vec{r}_i(0)-\vec{r}_i(t)\right)\rangle + \frac{1}{N}\langle\sum_{i\neq j}^{N}\delta\left(\vec{r}+\vec{r}_j(0)-\vec{r}_i(t)\right)\rangle$$

$$\equiv G_{\mathrm{s}}(\vec{r},t) + G_{\mathrm{d}}(\vec{r},t), \quad (4)$$

where the self part $G_{\mathrm{s}}(\vec{r},t)$ and the distinct part $G_{\mathrm{d}}(\vec{r},t)$ describe the average motions of the reference particle and the other $N-1$ particles, respectively.

Site analyses were performed by the site-analysis package [48]. A series of home-built scripts were used to parse the occupancy and average residence time of all the Li sites.

Concerted diffusion is a collective motion behavior, in which multiple ions hop simultaneously into their nearest sites within a short time interval [19]. The concerted diffusion mode analytical algorithm was performed to count for the process that the atom a moves from Site A to Site B, and atom b moves from Site B to Site C simultaneously within a time interval of 1 ps (referring to an attempt frequency of ~10^{12} Hz). Such a process is considered as an effective concerted diffusion process

along with the Site A–Site B–Site C diffusion pathway (Fig. S2).

2.3. First-principles calculations

The first-principles calculations based on density functional theory (DFT) were performed employing VASP. Perdew-Burke-Ernzerhof (PBE) exchange-correlation energy in the framework of generalized gradient approximation (GGA) was adopted [49]. The parameters in the first-principles calculations were set to be consistent with the setting in the Materials Project [38,50,51]. The ground-state structure of LGPS in [52] was adopted in our calculation.

The vacancy formation energy of Li, E_{f}, was determined as an indicator to evaluate the atomic bonding strength between Li atoms and neighbor GeS_4^{4-}/PS_4^{3-} tetrahedral frameworks,

$$E_{\mathrm{f}} = E_{\mathrm{vacancy}} + \mu_{\mathrm{Li}} - E_{\mathrm{perfect}}, \quad (5)$$

where E_{vacancy} and E_{perfect} are the total energies of the LGPS structure with a Li vacancy and a defect-free one, respectively. μ_{Li} is the chemical potential of Li atoms, which was set to the total energy per atom in the body-centered-cubic Li lattice.

3. Results and discussion

LGPS exhibits typical structural characteristics of SEs, where the liquid-like Li ions are randomly distributed in the crystallographic sites around GeS_4^{4-} and PS_4^{3-} tetrahedron frameworks (Scheme 1). The four Li sites were identified by the previous X-ray diffraction results, i.e., Li1(16*h*), Li2(4*d*), Li3(16*h*), and Li4(4*c*) [53]. An edge-shared tetrahedral chain of $[Li1]S_4$–$[Li1]S_4$–$[Li3]S_4$ forms the diffusion channel along the *c* axis, where the body-centered cubic-like anion framework is beneficial for the fast Li diffusion [54]. The in-plane *ab* diffusion channels are composed of $[Li2]S_6$–$[Li3]S_4$ and $[Li4]S_6$–$[Li1]S_4$ chains, while the Li ions at Li2 and Li4 sites hop slowly because of their six-coordination, especially for the Li2 site.

DPMD simulation is performed based on the following procedure (Scheme 1). First, high-quality data including atomic coordinates, energy, and force information are collected based on AIMD simulations of randomly disturbed LGPS structures. Second, coordinate-based descriptors are generated. Third, the descriptors are input into NNs to train an accurate potential energy surface (PES). Finally, MD simulations are performed based on the accurate PES.

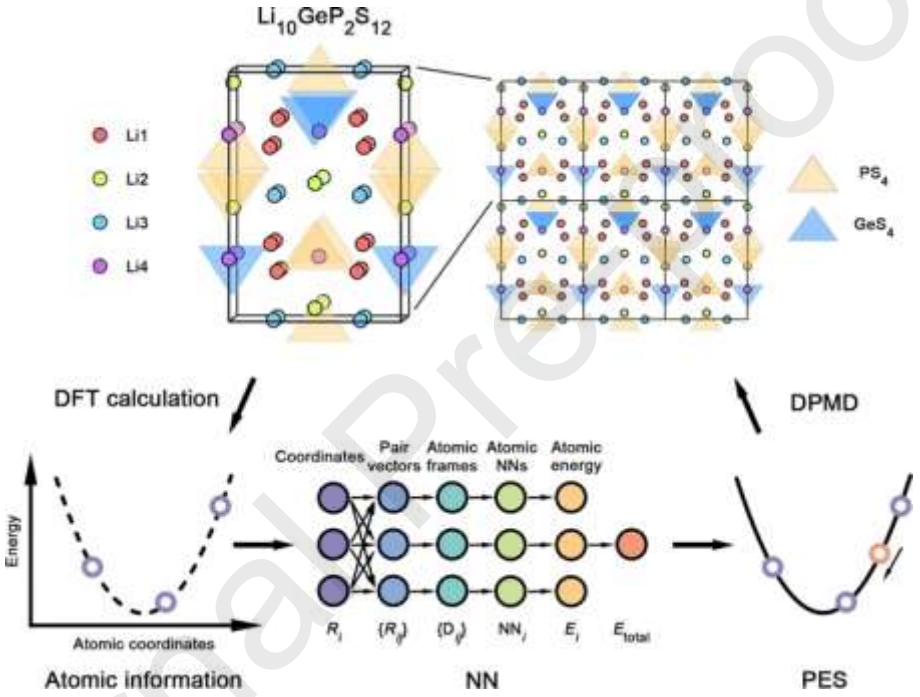

Scheme 1. Schematic of DPMD simulations. The technological process is divided into four steps: initial AIMD sampling, descriptor construction, NN training, and final DPMD production.

The ionic diffusivities of LGPS with different supercell sizes are firstly determined and compared (Figs. S3 and S4a) because of the size-dependent ionic diffusivities in MD simulations with periodic boundary conditions [55]. The ionic diffusivity is converged in a supercell with 900 atoms (i.e., a supercell of 3×3×2) (Fig. S4a), in agreement with previous results [42]. Therefore, the model with 900 atoms is

used in the following analysis.

The temperature-dependent Li ionic diffusivities in LGPS are revealed by both AIMD and DPMD simulations (Fig. 1a). Note that the simulation time of AIMD and DPMD is set to be 200 ps and 40 ns, respectively. DPMD simulations deliver Arrhenius-type temperature dependence of ionic diffusivity within a wide temperature range from 250 to 1200 K, in agreement with the previous high-temperature AIMD simulations [19,56,57]. An activation energy of 0.23 eV is further determined based on the Arrhenius-type temperature dependence, very close to the previous AIMD (0.21 ± 0.01 [56] and 0.23 ± 0.03 [19]) and experimental (0.24 eV [8]) results. Especially, a room-temperature ionic diffusivity of 7.1×10^{-12} m^2s^{-1} determined by DPMD simulations is close to the experimental result ($4.1 \pm 2 \times 10^{-12}$ m^2s^{-1} [58]), in contrary to that of 1.3×10^{-10} m^2s^{-1} by AIMD simulations. The accuracy improvement on ionic diffusivity by DPMD simulations is attributed to its longer simulation time and larger simulation size at low temperatures to ensure a sufficient diffusion event sampling compared with sampling-limited AIMD simulations (Fig. S5) [56].

The Arrhenius-type temperature dependence in LGPS rationalizes the linear extrapolation of high-temperature AIMD simulations, which can afford a fairly precise ionic diffusivity of LGPS at room temperature [56]. However, the empirically linear extrapolation of AIMD simulation will fail in the SEs with the non-Arrhenius temperature dependence of the ionic diffusivities due to the large prediction deviation at low temperatures, which can be decently addressed by DPMD.

In order to reveal the underlying Li-ion diffusion mechanism in LGPS, the temperature-dependent anisotropy of the Li ionic diffusivities is determined to decompose the contribution of the Li-ion diffusion along the two diffusion channels.

The contribution of the in-place *ab* component to the total ionic diffusivity increases monotonously with the temperature (Fig. 1b) except for an abnormal point at 300 K. The comparison in different simulation sizes validates the statistically abnormal contribution at 300 K (Fig. S4b).

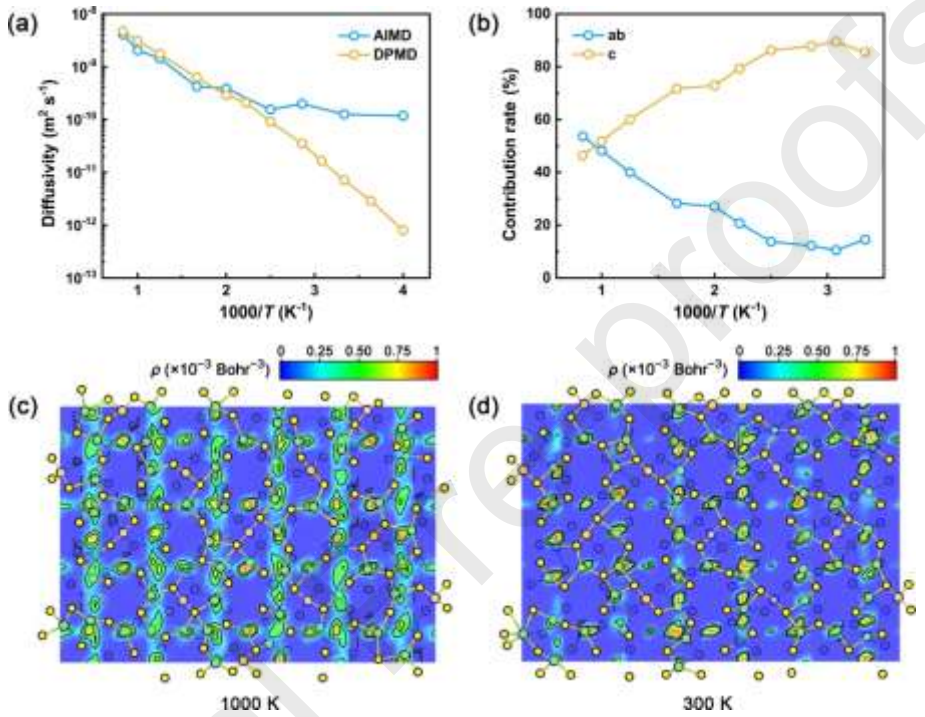

Fig. 1. Diffusion behavior in the LGPS lattice. (a) Arrhenius plot in LGPS simulated with both AIMD and DPMD. (b) The dimensional contribution of Li-ion diffusion in LGPS as a function of inverse temperature. Li-ion probability densities ρ in LGPS at (c) 1000 and (d) 300 K.

A continuous distribution of Li probability density along the diffusion pathway is perceived at 1000 K (Fig. 1c, Figs. S6a, c, and e), implying more frequent diffusion events and more comparable diffusion and residence time at higher temperatures. It is different from the distinct Li probability density localization at the stable crystallographic sites at 300 K (Fig. 1d, Figs. S6b, d, and f). Flatter radial distribution

functions for Li–Li and Li–S pairs at 1000 K compared to that at 300 K indicate a more disordered Li distribution at higher temperatures (Fig. S7).

A dominant concerted diffusion mechanism has been widely reported to explain the fast Li-ion conduction in LGPS [19]. Haven ratio and Van Hove correlation function are usually used to quantitatively describe the concerted diffusion. The Haven ratio H_R is the ratio of tracer ionic diffusivity D^* to charge ionic diffusivity D_σ (formula 6),

$$H_R = \frac{D^*}{D_\sigma}, \quad (6)$$

which describes the average correlation strength of ionic motions in lattices [45]. A temperature-independent H_R of 0.42 in LGPS [59] indicates a similar correlation strength of ionic motions at different temperatures, i.e., a similar ratio of concerted ionic motions to total diffusion motions. Similar temperature-independent H_R was found in Li_6PS_5Cl [60], doped ceria $Ce_{0.9}Gd_{0.1}O_{1.95}$ [61], AgI [62], amorphous Li_3PO_4 [63], and $0.2Na_2O•0.8B_2O_3$ glass [64].

Van Hove correlation function analyses were further performed to reveal the concerted diffusion in LGPS. Similar red peaks appear at r=0 in the distinct parts of the Van Hove correlation functions at 300 and 1000 K (Fig. S8), indicating the position of the reference Li ions is occupied by other Li ions, which is the evidence of correlation motions [16]. A shorter characteristic time (1 ps) at 1000 K compared to that (30 ps) at 300 K suggests more frequent concerted diffusion events at higher temperatures [15].

To provide a quantitative site analysis of the concerted diffusion mechanism in LGPS, the Voronoi decomposition is adopted to divide the lattice space into sites (Fig. 2a) [65] and the occupancy information of each site can be further derived from the MD trajectory. The occupancy information of 576 Li sites within a simulation time of

1 ns at different temperatures is collected and shown as heatmaps (Fig. 2b–d and Fig. S9). The more frequent occupied (blue)–unoccupied (white) transitions along the time axis at higher temperatures imply more motion events and the shorter site residence time, in agreement with the results of the Van Hove correlation function analyses. The distinct Li-ion site occupancy distribution at 300 K becomes disordered at 1000 K, especially in the Li1–Li3–Li1 diffusion channel (Fig. 2b), which indicates liquid-like Li ion motion behaviors at high temperatures.

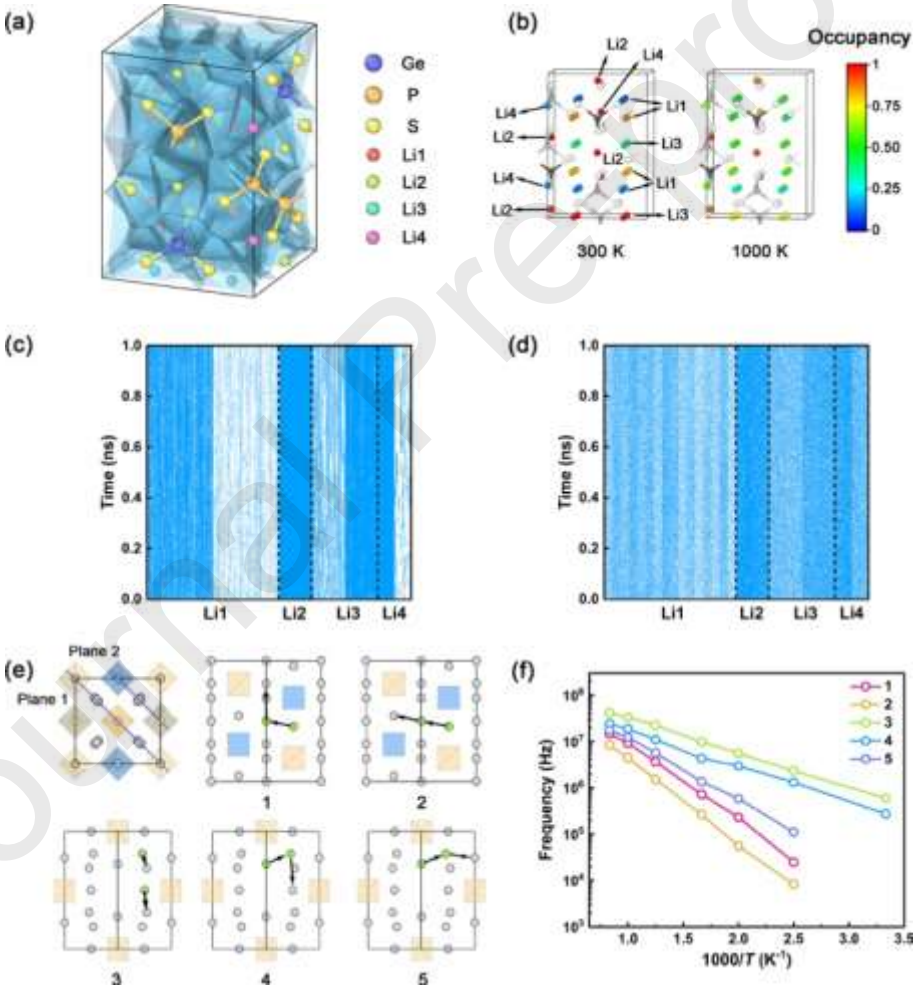

Fig. 2. Diffusion mechanism in LGPS. (a) Schematic of a Voronoi decomposition of the LGPS lattice. (b) The time-averaged Li site occupancy ratio in LGPS at 300 and 1000 K. The time evolution of Li site occupancy at (c) 300 and (d) 1000 K, in which

the blue and white grid points denote the occupied and unoccupied states, respectively. (e) Five possible concerted diffusion modes in the (110) plane, in which Types 1–2 and 3–5 are located in Planes 1 and 2, respectively. The positional relationship of the two planes is shown at the top left corner of the subfigure. (f) The jump frequency of the concerted diffusion modes as a function of inverse temperature.

Based on the site occupancy information, the jump frequency of concerted diffusion modes at different temperatures can be further obtained (Fig. S2). The two-atom concerted diffusion modes can be divided into five classes (Fig. 2e), including Li2–Li3–Li1 (Type 1), Li2–Li3–Li2 (Type 2), Li1–Li3–Li1 (Type 3), Li4–Li1–Li3 (Type 4) and Li4–Li1–Li4 (Type 5). All jump frequencies of the concerted diffusion modes exhibit linear temperature dependences (Fig. 2f), agreeing with the Arrhenius plot of ionic diffusivity against temperature (Fig. 1a). If the collective ionic jumps are regarded as thermally activated Brownian motion, the jump frequency v can be expressed as follows [45]:

$$v = v_0 \exp\left(-\frac{\Delta G}{k_B T}\right) = v_0 \exp\left(\frac{\Delta S}{k_B}\right) \exp\left(-\frac{\Delta H}{k_B T}\right), \quad (7)$$

where v_0 is the attempt frequency, k_B is the Boltzmann constant, T is the temperature, ΔG is the Gibbs free energy of activation, ΔS is the activation entropy, and ΔH is the activation enthalpy (i.e., approximate activation energy at the ambient condition). The activation energies of all concerted diffusion modes are further determined based on the linear relationship between the jump frequencies and the inverse temperature, that is, 0.33, 0.36, 0.15, 0.15, and 0.26 eV for Types 1–5, respectively, consistent with the activation energies (0.18, 0.17, and 0.37 eV for Types 3–5, respectively) determined by DFT calculations [66]. The similar activation energies of the concerted diffusion modes between the DFT calculation at 0 K and our DPMD simulation at finite

temperature imply the temperature-independent PES of the Li-ion diffusion.

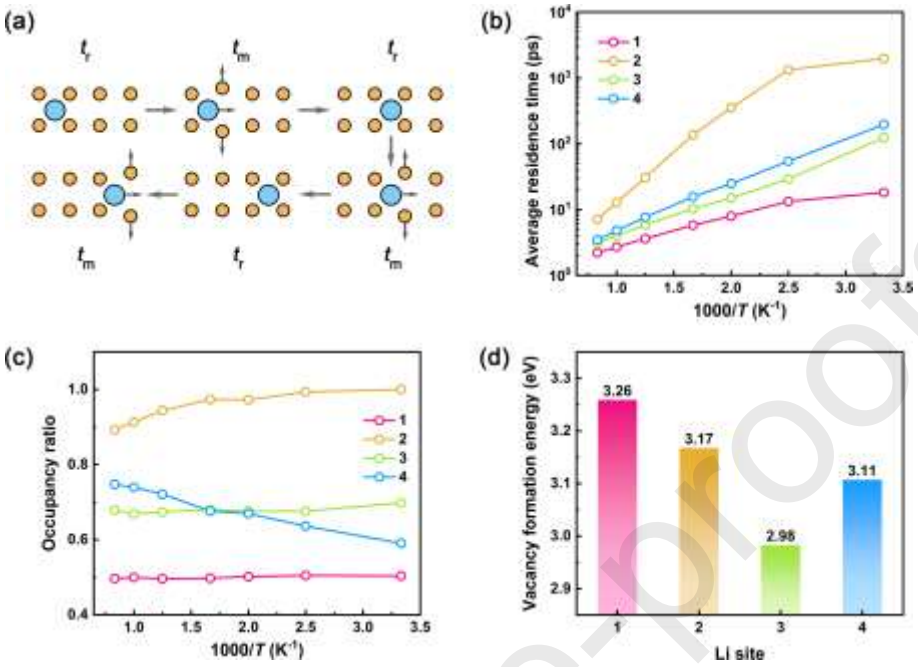

Fig. 3. Li site analyses in LGPS. (a) Schematic of residence time t_r and migration time t_m for a mobile ion. (b) Averaged residence time and (c) site occupancy ratio regarding the Li atoms at four Li sites as a function of inverse temperature. (d) Li vacancy formation energy averaged by Li sites in LGPS lattice.

Similar to the jump frequency of Li ions, the averaged residence time (t_r) for the Li ions at four sites is further determined to reveal the concerted diffusion mechanisms. There exist two states, i.e., vibration and migration (Fig. 3a), for Li ions in lattices. Therefore, the time can be accordingly divided into residence and migration time (t_m). The latter can be ignored because it is usually much shorter than the former. The linear temperature dependence of the averaged residence time is observed except for the slight deviation at 300 K due to the insufficient sampling time of 2 ns (Fig. 3b). The significant decrease of the average residence time for the Li ions at the Li2 site with an increasing temperature indicates the temperature-dependent

thermal activation of the Li atoms at the Li2 site, which is usually regarded as an inactive site at low temperatures [67,68]. The site occupancies of four Li sites are further determined to explore the origin of the activation of the Li ions at the Li2 site under elevated temperatures (Fig. 3c). The occupancy ratio of the Li2 site ranges from 1 at 300 K to 0.91 at 1000 K, suggesting the increasing number of unoccupied Li2 sites is responsible for the increasing Li2 site-related diffusion behavior.

A correlation of Li-ion diffusion barriers with binding strengths between Li and neighbor atoms in LGPS was found in our previous work [52]. An additional DFT calculation is performed to determine the vacancy formation energy of Li sites, which is considered as an indicator of the atomic binding strengths [52]. Similar vacancy formation energies (3.17 and 3.11 eV) for the Li atoms at Li2 and Li4 sites imply a similar atomic binding strength at two sites and are supposed to further imply a similar diffusion barrier for Li2- and Li4-related diffusion modes (Fig. 3d). The evaluation is conflicting with the lower activation energies of the concerted diffusion modes across the Li4 site than that of the modes across the Li2 site, indicating the changed PES of Li-ion diffusions by concerted diffusions. Deviating from the fundamental assumption of individual ion motions and neglected interactions between mobile ions in the classical diffusion model, the interactions between mobile ions need to be considered for a reasonable PES in the concerted diffusion model. A significantly reduced activation energy of 0.2–0.4 eV in LLZO was demonstrated by a multi-ion concerted diffusion model [19], highlighting the dominating role of the cooperative effect on Li-ion diffusion in SEs.

Over decades, concerted diffusion has been believed to be the origin of fast ion diffusion in SEs [19]. However, understanding concerted diffusion modes in SEs and developing a quantitative model of ion transport in SEs are very challenging.

Although the transition state model of multi-ion concerted diffusion has been established and demonstrated decreased diffusion barrier, concerted diffusion modes are difficult to be quantitatively characterized by conventional experimental and computational methods. Even though AIMD can simulate the high-temperature behaviors of ionic motions in a limited simulation size, it is far away from a fundamental understanding of ionic motions based on the following reason: (1) Low-temperature and long-time simulations are necessary due to the varied diffusion mechanisms at low and high temperatures for some SEs; (2) Frequent and interlocking ionic motions at high temperature create extra obstacles to evaluate the cooperative motion behaviors. Since it is extremely difficult to accurately fit temperature-dependent empirical parameters in CMD, a significant accuracy deviation is achieved in CMD simulation to probe the response of ionic transport to temperature. Such an issue is elaborately addressed by the empirical-parameter-free DPMD simulation. The DPMD method established in this study provides an effective approach to perform a large-scale, long-time, and room-temperature simulation and directly probe the behaviors of ionic concerted diffusions in SEs (Movies S1–S2), which is of great concern to understand the ionic diffusion mechanism in SEs.

LGPS is chosen as a prototype to understand the ionic diffusion mechanism in SEs. Several new findings are summarized and listed below. (1) Reasonable Li-ion diffusion pathways and decreased residence time of Li sites at high temperature are effectively recognized, coincident with the previous nuclear magnetic resonance results [22,69]. (2) Collective motions of Li ions dominantly contribute to Li-ion transports in LGPS at both low and high temperatures, suggesting the lower activation energy of concerted diffusions compared to that of a single ion jump. Such a finding strongly confirms the results predicted by DFT calculations [19]. (3) The concerted

diffusion mode Li4–Li1–Li3 containing both in-plane and out-of-plane components is directly extracted from the MD simulations for the first time. The derived activation energy (0.15 eV) of the Li1–Li3–Li4 mode is in excellent agreement with the previous DFT calculation result (0.17 eV) [66], indicating the non-negligible contribution of in-place diffusion to the total Li-ion transport. Such finding is a possible origin of a weak anisotropic ionic conductivity in a single-crystal LGPS [53].

The new insight into the temperature-dependent concerted ionic diffusion mechanism in LGPS is of both fundamental significance to the understanding of the ion transport mechanism in SEs and practical guidance to the rational design of advanced SEs with high ionic conductivities. First, the Arrhenius correlation between ionic diffusivity and temperature ranging from 250 to 1200 K highlights the important role of MLMD simulations in probing ion transport mechanisms in SEs. Second, the concerted ionic diffusion mechanism is originated from the Li–Li interactions between high- and low-energy sites. Similar to temperature, other strategies are also able to change the Li ion distribution and enhance such Li–Li interactions. For example, the introduction of heteroatoms can destroy the symmetry of PES and induce a more disordered distribution of Li ions. A disordered Li ion distribution is beneficial to enhance the Li–Li interactions between high- and low-energy sites and consequently activate the concerted ionic diffusion mechanism. Third, the design strategy discussed above for bulk SEs applies to the interface design. The interfacial engineering and the nanonization of particles can regulate the concerted ionic diffusion mechanism and therefore promote the ion transport at the interface.

4. Conclusions

The temperature-dependent concerted diffusion behaviors in LGPS are comprehensively investigated by advanced DPMD simulations. The temperature

dependence of Li ionic diffusivities exhibits an Arrhenius behavior ranging from 250 to 1200 K, which is attributed to the dependence of jump frequencies of various concerted diffusion modes on the temperature. The degree of the ordering of Li ions, averaged residence time for the Li ions at four Li sites, Li-ion probability density, and diffusion anisotropy in LGPS are regulated by temperature. Li2-related concerted diffusion modes are observed at high temperatures due to the occupancy change of Li2 sites although the Li2 site is usually regarded as an inactive site. These findings afford a fundamental understanding of the temperature-dependent ionic diffusion mechanism in SEs and are helpful to discover the working mechanism of solid-state batteries at all relevant temperatures.

Acknowledgments

This work was supported by the National Key Research and Development Program (2021YFB2500210), the Beijing Municipal Natural Science Foundation (Z20J00043), the National Natural Science Foundation of China (22109086 and 21825501), the China Postdoctoral Science Foundation (2021TQ0161 and 2021M691709), and the Guoqiang Institute at Tsinghua University (2020GQG1006). X. Chen appreciates the support from the Shuimu Tsinghua Scholar Program of Tsinghua University. The authors acknowledged the support from Tsinghua National Laboratory for Information Science and Technology for theoretical simulations.

References

[1] J.B. Boyce, B.A. Huberman, Phys. Rep. 51 (1979) 189–265.

[2] J.B. Goodenough, Proc. R. Soc. Lond. A 393 (1984) 215–234.

[3] Y. Lu, C.-Z. Zhao, R. Zhang, H. Yuan, L.-P. Hou, Z.-H. Fu, X. Chen, J.-Q. Huang, Q. Zhang, Sci. Adv. 7 (2021) eabi5520.

[4] S. Sun, D. Rao, T. Zhai, Q. Liu, H. Huang, B. Liu, H. Zhang, L. Xue, H. Xia,

Adv. Mater. 32 (2020) 2005344.

[5] R. Murugan, V. Thangadurai, W. Weppner, Angew. Chem. Int. Ed. 46 (2007) 7778–7781.

[6] H. Aono, E. Sugimoto, Y. Sadaoka, N. Imanaka, G.Y. Adachi, J. Electrochem. Soc. 137 (1990) 1023–1027.

[7] Y. Inaguma, C. Liquan, M. Itoh, T. Nakamura, T. Uchida, H. Ikuta, M. Wakihara, Solid State Commun. 86 (1993) 689–693.

[8] N. Kamaya, K. Homma, Y. Yamakawa, M. Hirayama, R. Kanno, M. Yonemura, T. Kamiyama, Y. Kato, S. Hama, K. Kawamoto, A. Mitsui, Nat. Mater. 10 (2011) 682–686.

[9] H.-J. Deiseroth, S.-T. Kong, H. Eckert, J. Vannahme, C. Reiner, T. Zaiß, M. Schlosser, Angew. Chem. Int. Ed. 47 (2008) 755–758.

[10] F. Mizuno, A. Hayashi, K. Tadanaga, and M. Tatsumisago, Adv. Mater. 17 (2005) 918–921.

[11] Y. Seino, T. Ota, K. Takada, A. Hayashi, M. Tatsumisago, Energy Environ. Sci. 7 (2014) 627–631.

[12] T. Asano, A. Sakai, S. Ouchi, M. Sakaida, A. Miyazaki, S. Hasegawa, Adv. Mater. 30 (2018) 1803075.

[13] T. Famprikis, P. Canepa, J.A. Dawson, M.S. Islam, C. Masquelier, Nat. Mater. 18 (2019) 1278-1291.

[14] J.C. Bachman, S. Muy, A. Grimaud, H.-H. Chang, N. Pour, S.F. Lux, O. Paschos, F. Maglia, S. Lupart, P. Lamp, L. Giordano, Y. Shao-Horn, Chem. Rev. 116

(2016) 140–162.

[15] W. Kob, C. Donati, S.J. Plimpton, P.H. Poole, S.C. Glotzer, Phys. Rev. Lett. 79 (1997) 2827–2830.

[16] C. Donati, J.F. Douglas, W. Kob, S.J. Plimpton, P.H. Poole, S.C. Glotzer, Phys. Rev. Lett. 80 (1998) 2338–2341.

[17] G.E. Murch, Solid State Ion. 7 (1982) 177–198.

[18] M. Burbano, D. Carlier, F. Boucher, B.J. Morgan, M. Salanne, Phys. Rev. Lett. 116 (2016) 135901.

[19] X. He, Y. Zhu, Y. Mo, Nat. Commun. 8 (2017) 15893.

[20] J.G. Smith, D.J. Siegel, Nat. Commun. 11 (2020) 1483.

[21] Z. Zhang, H. Li, K. Kaup, L. Zhou, P.-N. Roy, L.F. Nazar, Matter 2 (2020) 1667–1684.

[22] D.A. Weber, A. Senyshyn, K.S. Weldert, S. Wenzel, W. Zhang, R. Kaiser, S. Berendts, J. Janek, W.G. Zeier, Chem. Mater. 28 (2016) 5905–5915.

[23] A.D.G. Truhlar, B.C. Garrett, Annu. Rev. Phys. Chem. 35 (1984) 159–189.

[24] B.J. Morgan, Philos. Trans. Royal Soc. A 379 (2021) 20190451.

[25] M.T. Dove, Introduction to lattice dynamics, Cambridge University Press, Cambridge, 1993.

[26] O.T. Unke, S. Chmiela, H.E. Sauceda, M. Gastegger, I. Poltavsky, K.T. Schütt, A. Tkatchenko, K.-R. Müller, Chem. Rev. 121 (2021) 10142–10186.

[27] J. Qi, S. Banerjee, Y. Zuo, C. Chen, Z. Zhu, M.L. Holekevi Chandrappa, X. Li, S.P. Ong, Mater. Today Phys. 21 (2021) 100463.

[28] J. Behler, Chem. Rev. 121 (2021) 10037–10072.

[29] L. Zhang, J. Han, H. Wang, R. Car, W. E, Phys. Rev. Lett. 120 (2018) 143001.

[30] X. Chen, X. Liu, X. Shen, Q. Zhang, Angew. Chem. Int. Ed. 60 (2021) 24354–24366.

[31] P.B. Calio, C. Li, G.A. Voth, J. Am. Chem. Soc. 143 (2021) 18672–18683.

[32] L. Zhang, H. Wang, R. Car, W. E, Phys. Rev. Lett. 126 (2021) 236001.

[33] M. Galib, D.T. Limmer, Science 371 (2021) 921–925.

[34] Y. Zhang, H. Wang, W. Chen, J. Zeng, L. Zhang, H. Wang, W. E, Comput. Phys. Commun. 253 (2020) 107206.

[35] G. Kresse, J. Furthmüller, Phys. Rev. B 54 (1996) 11169–11186.

[36] H. Wang, L. Zhang, J. Han, W. E, Comput. Phys. Commun. 228 (2018) 178–184.

[37] S. Plimpton, J. Comput. Phys. 117 (1995) 1–19.

[38] A. Jain, S.P. Ong, G. Hautier, W. Chen, W.D. Richards, S. Dacek, S. Cholia, D. Gunter, D. Skinner, G. Ceder, K.A. Persson, APL Mater. 1 (2013) 011002.

[39] A. Kuhn, V. Duppel, B.V. Lotsch, Energy Environ. Sci. 6 (2013) 3548–3552.

[40] G. Kresse, J. Hafner, Phys. Rev. B 47 (1993) 558–561.

[41] A. Marcolongo, T. Binninger, F. Zipoli, T. Laino, ChemSystemsChem 2 (2020) e1900031.

[42]J. Huang, L. Zhang, H. Wang, J. Zhao, J. Cheng, W. E, J. Chem. Phys. 154 (2021) 094703.

[43] S. Nosé, J. Chem. Phys. 81 (1984) 511–519.

[44] W.G. Hoover, Phys. Rev. A 31 (1985) 1695–1697.

[45] Y. Gao, A.M. Nolan, P. Du, Y. Wu, C. Yang, Q. Chen, Y. Mo, S.-H. Bo, Chem. Rev. 120 (2020) 5954–6008.

[46] Z. Deng, Z. Zhu, I.-H. Chu, S.P. Ong, Chem. Mater. 29 (2017) 281–288.

[47] S.P. Ong, W.D. Richards, A. Jain, G. Hautier, M. Kocher, S. Cholia, D. Gunter, V.L. Chevrier, K.A. Persson, G. Ceder, Comput. Mater. Sci. 68 (2013) 314–319.

[48] B.J. Morgan, site-analysis, https://github.com/bjmorgan/site-analysis.

[49] J.P. Perdew, K. Burke, M. Ernzerhof, Phys. Rev. Lett. 77 (1996) 3865–3868.

[50] A. Jain, G. Hautier, C.J. Moore, S. Ping Ong, C.C. Fischer, T. Mueller, K.A. Persson, G. Ceder, Comput. Mater. Sci. 50 (2011) 2295–2310.

[51] A. Jain, G. Hautier, S.P. Ong, C.J. Moore, C.C. Fischer, K.A. Persson, G. Ceder, Phys. Rev. B 84 (2011) 045115.

[52] Z.-H. Fu, X. Chen, C.-Z. Zhao, H. Yuan, R. Zhang, X. Shen, X.-X. Ma, Y. Lu, Q.-B. Liu, L.-Z. Fan, Q. Zhang, Energy Fuels 35 (2021) 10210–10218.

[53] R. Iwasaki, S. Hori, R. Kanno, T. Yajima, D. Hirai, Y. Kato, Z. Hiroi, Chem. Mater. 31 (2019) 3694–3699.

[54] Y. Wang, W.D. Richards, S.P. Ong, L.J. Miara, J.C. Kim, Y. Mo, G. Ceder, Nat. Mater. 14 (2015) 1026–1031.

[55] I.-C. Yeh, G. Hummer, J. Phys. Chem. B 108 (2004) 15873–15879.

[56] X. He, Y. Zhu, A. Epstein, Y. Mo, npj Comput. Mater. 4 (2018) 18.

[57] Y. Mo, S.P. Ong, G. Ceder, Chem. Mater. 24 (2012) 15–17.

[58] A. Kuhn, J. Köhler, B.V. Lotsch, Phys. Chem. Chem. Phys. 15 (2013) 11620–11622.

[59] A. Marcolongo, N. Marzari, Phys. Rev. Mater. 1 (2017) 025402.

[60] P. Adeli, J.D. Bazak, K.H. Park, I. Kochetkov, A. Huq, G.R. Goward, L.F. Nazar, Angew. Chem. Int. Ed. 58 (2019) 8681–8686.

[61] S. Grieshammer, I.V. Belova, G.E. Murch, Acta Mater. 210 (2021) 116802.

[62] H. Okazaki, J. Phys. Soc. Jpn. 23 (1967) 355–360.

[63]N. Kuwata, X. Lu, T. Miyazaki, Y. Iwai, T. Tanabe, J. Kawamura, Solid State Ion. 294 (2016) 59–66.

[64] Á.W. Imre, H. Staesche, S. Voss, M.D. Ingram, K. Funke, H. Mehrer, J. Phys. Chem. B 111 (2007) 5301–5307.

[65] B.J. Morgan, Chem. Mater. 33 (2021) 2004–2018.

[66] A. Bhandari, J. Bhattacharya, J. Phys. Chem. C 120 (2016) 29002–29010.

[67] Y. Kato, S. Hori, R. Kanno, Adv. Energy Mater. 10 (2020) 2002153.

[68] Y. Kato, S. Hori, T. Saito, K. Suzuki, M. Hirayama, A. Mitsui, M. Yonemura, H. Iba, R. Kanno, Nat. Energy 1 (2016) 16030.

[69] X. Liang, L. Wang, Y. Jiang, J. Wang, H. Luo, C. Liu, J. Feng, Chem. Mater. 27 (2015) 5503-5510.

Graphical abstract

Concerted diffusions of ions in solid electrolytes are probed through machine-learning molecular dynamics simulation, which are beneficial to understand fast Li-ion conduction in solid electrolytes.